Journal of Catalysis 271 (2010) 228–238

Contents lists available at ScienceDirect

Journal of Catalysis

journal homepage: www.elsevier.com/locate/jcat

Effects of CO_2 and steam on Ba/Ce-based NO_x storage reduction catalysts during lean aging

Ming Yang [a], Yuping Li [b], Jun Wang [a], Meiqing Shen [a,c,*]

[a] Key Laboratory for Green Chemical Technology of State Education Ministry, School of Chemical Engineering & Technology, Tianjin University, Tianjin 300072, PR China
[b] Troy Athens High School, Troy, Michigan 48085, USA
[c] State Key Laboratory of Engines, Tianjin University, Tianjin 300072, PR China

ARTICLE INFO

Article history:
Received 10 September 2009
Revised 12 January 2010
Accepted 18 January 2010
Available online 13 February 2010

Keywords:
NO_x storage reduction
Aging
Barium cerate
Barium carbonate
Ceria
Support oxides

ABSTRACT

The effects of CO_2 and steam on the morphological and chemical properties of Ba/Ce-based NO_x storage reduction (NSR) catalysts during the aging were investigated. At 800 °C, $BaCeO_3$ formation was prevented by a CO_2 concentration as low as 5%, which shows little effect on suppressing $BaAl_2O_4$ and $BaZrO_3$ formation. CO_2 protects hexagonal $BaCO_3$, BaO_2, and CeO_2, to form $BaCeO_3$, by increasing one time higher activation energy for decarbonation, and maintaining orthorhombic $BaCO_3$ as the most stable storage component. Steam accelerates the particle aggregations, but it does not determine the above chemical equilibrium. In NSR reactions, although $BaCeO_3$ formation can be excluded in an atmosphere containing CO_2, the nitrite/nitrate bonding stabilization and the complete NO_x reduction are hindered by the highly crystallized materials (induced by higher CO_2 and/or steam concentrations during aging). Particle aggregation is a major factor responsible for the deactivation of the aged Ba/Ce-based NSR catalysts.

1. Introduction

Lean NO_x trap (LNT), also known as NO_x storage reduction (NSR), has drawn wide attention as an advanced exhaust control technology to reduce NO_x emissions from lean-burn engines [1]. A typical NSR catalyst formulation contains basic NO_x storage components (mostly barium species), noble metals (NM, such as Pt, Rh, Pd), and support oxides. The combined effects of these three components efficiently remove NO_x from vehicle exhaust through the periodic operations of NO_x oxidation, NO_x sorption, NO_x release, and NO_x reduction [2,3].

Ceria-based materials have been shown to be beneficial for NSR catalysts. They maintain higher metal dispersions [4], provide surface basicity to benefit the formation of carbonates [5], promote the water–gas shift (WGS) reaction and the reduction of NO_x at anionic vacancies [6], and release lattice oxygen, which modifies the redox process [7]. Many current commercial samples have already incorporated ceria into NO_x traps. Several research articles have reported the outstanding performance of Ba/Ce-based NSR catalysts compared to the catalysts with other oxide supports (Al, Si, or Zr), although ceria-based materials are admitted to have several drawbacks [3,8,9]. Not only do ceria-based materials sinter at relatively low temperatures [3], they also maintain the oxidation states of NM during rich periods [10], and their surface basicity is negative for NO oxidation in lean conditions [11].

Thermal deterioration, especially with concern to the modification of NO_x storage components [12], is one of the main reasons for the deactivation of NSR catalysts [2]. Besides several recent studies focused on the Pt–Ba interactions [13,14], much emphasis is put on the barium-based components modified by the Ba-support interactions [2,3]. The formation of $BaCeO_3$, $BaAl_2O_4$, and $BaZrO_3$ in Ba/Ce, Ba/Al, and Ba/Zr systems is well documented, and these compounds are known to decrease the NO_x storage efficiency [9,15]. Additionally, investigations into the regeneration of thermal-aged NSR catalysts have been reported [12,15]. In general, treatments in an acidic liquid (water) or a 300–800 °C acidic atmosphere, in which H_2O, NO_x, and CO_2 are applied at concentrations much higher than those in the exhaust, are required for the regenerations. Therefore, it is desirable to develop a heterogeneous NSR catalyst that does not form the inactive phases during the aging treatment or readily regenerates the deactivated phases under realistic conditions in vehicle exhaust [2]. Regeneration of $BaCeO_3$ is more likely when compared with that of $BaAl_2O_4$ and $BaZrO_3$ [15]. However, the possibility of $BaCeO_3$ formation under realistic applications was questioned due to the lower concentrations of CO_2 and H_2O

* Corresponding author. Address: School of Chemical Engineering and Technology, Tianjin University, 92 Weijin Road, Nankai District, Tianjin 300072, China. Fax: +86 22 27892301.
E-mail address: mqshen@tju.edu.cn (M. Shen).

0021-9517/$ - see front matter © 2010 Elsevier Inc. All rights reserved.
doi:10.1016/j.jcat.2010.01.018

Table 1
Descriptions of the different aging treatments.

Names of the treatments	Brief description (for 0–18 h aging)
Fresh	As-prepared samples
Thermal	Samples treated in 800 °C air
Hydrothermal	Samples treated at 800 °C in 10% steam (air balance)
5%* CO_2 thermal	Samples treated at 800 °C in 5% CO_2 (air balance)
10% CO_2 thermal	Samples treated at 800 °C in 10% CO_2 (air balance)
5% CO_2 hydrothermal	Samples treated at 800 °C in 5% CO_2 + 10% steam (air balance)
10% CO_2 hydrothermal	Samples treated at 800 °C in 10% CO_2 + 10% steam (air balance)

* All percentages presented stand for gaseous percentages in volume.

(NO_x can be eliminated) found in lean-burn exhaust [12]. It is not clear whether the decent activity of Ba/Ce-based NSR catalysts is due to the higher NO_x storage capacity (NSC) of $BaCeO_3$, or the improved maintenance of active phases against $BaCeO_3$.

The performance of the aged NSR catalysts strongly depends on the real operation conditions; and therefore, the lab aging strategies should be careful examined. Even at similar temperatures, different atmospheric compositions during the aging treatments will have a significant impact on the aged catalyst performance [5,16]. In contrast to the periodically varying NO_x concentrations (eliminated at most of the time), the concentrations of CO_2 and steam are kept almost at a constant level during the lean–rich cycles. Their continuous effects of modifying NSR materials should be studied.

Temperature-dependent effects of steam and CO_2 during NSR reactions have been systematically studied [5,16], but their influences during long time aging have yet to be thoroughly investigated. In the present work, the effects of CO_2 and steam on the morphological and chemical properties of Ba/Ce-based NO_x NSR materials during the aging treatments were studied through surface/bulk analysis and activity tests. Since there is little evidence that noble metals change the Ba-support interaction [13,17], the NM-related interactions have been decoupled from the Ba–Ce contact for most of the samples we investigated.

2. Experimental

2.1. Sample preparation

For the supported samples, Pt and BaO were loaded by wet impregnation, using $Pt(NO_3)_2$ and $Ba(Ac)_2$ solutions, respectively. CeO_2, Al_2O_3, and ZrO_2 support oxides were from Aldrich. The impregnated materials were calcined in air at 500 °C for 5 h to obtain the fresh samples. Only the BaO/CeO_2 parts were treated under different aging conditions, and they were mixed with the fresh 2 wt.% Pt/Al_2O_3 in the weight ratio of 6:4 right before the catalytic tests. For comparison, 2 wt.% Pt/30 wt.% BaO/CeO_2 samples and 30 wt.% BaO/2 wt.% Pt/CeO_2 samples were also prepared (Pt and Ba impregnated with reverse sequences), in which the NM and barium species were loaded on the same support oxide in reverse sequences. Descriptions of the different treating strategies are listed in Table 1.

Pertaining to the impregnated BaO/CeO_2 samples, the contact between barium species and ceria takes place on the interface where the barium salts were wet-impregnated. According to our X-ray diffraction and thermogravimetric data, the insufficient close Ba–Ce contact and less barium content make the quantification of the major phases and the tracking of the minor intermediate species difficult. Therefore, co-precipitated Ba/Ce (molar ratio 1:1) mixed compounds magnifying the Ba–Ce close contact, designated as BaCe11, were used in the study for comparison. The BaCe11 samples were prepared by adding $Ce(NO_3)_3 \cdot 6H_2O$ and $Ba(NO_3)_3$ into a NH_4HCO_3 precipitator. Additional basic solutions were added until pH = 9 (200% in excess). The precipitates were stirred at room temperature (RT) for 30 minutes and stabilized at 60 °C for 12 h. After being filtered and washed with de-ionized water till pH = 7, the products were dried at 100 °C for 12 h. Fresh powders were obtained after the subsequent calcination in air at 500 °C for 5 h. The majority of fresh powder is able to be converted into $BaCeO_3$ crystallites after 4 h calcination at 1100 °C according to XRD analysis [18,19].

2.2. Characterization and model reaction

The XRD patterns were acquired using X'Pert Pro diffractometer operating at 30 kV and 30 mA with nickel-filtered Co Kα radiation, at a 0.02° step size. For *in situ* experiments, the heating rate from RT to the target temperature was 10 °C/min, and the space velocity was 10,000 h^{-1}. Percentages of detected crystallites in samples were estimated by comparing the obtained XRD patterns with the monocomponents patterns of standardized crystallites in HIGHSCORE software database. Crystal sizes are calculated by JADE 5. Thermogravimetric experiments were conducted on METTLER TOLEDO TGA/DSC 1. Approximately, 20 mg of fresh sample was heated in a gas flow (50 ml/min) at a heating rate of 5, 10, and 15 °C/min, respectively.

BET surface areas were measured using N_2 adsorption with a Quantachrome NOVA 1200. Scanning electron microscopy (SEM) of the samples coated with Au–Pd was measured on a HITACHI S4800 field emission microscope. X-ray energy dispersive spectroscopy (EDS, NORAN System 7) results indicated that the enrichment of $BaCO_3$ generally shows deep color, CeO_2 the intermediate, and $BaCeO_3$ the light color.

In situ DRIFTS of NO_x isothermal adsorption and temperature programmed desorption were performed on a NICOLET 6700 FT-IR equipped with a commercial reaction chamber (Thermofisher) at the resolution of 1 cm^{-1}. Ten scans were operated for each spectrum. Powder samples were purged in 0.3% O_2/N_2 balance from RT to 500 °C. The sample cell was then cooled to 350 °C under the same atmosphere. NO_x adsorption measurements were conducted by introducing freshly mixed 0.075% NO/0.3% O_2/N_2 balance to the chamber at 350 °C. After the saturation of NO_x adsorption, which was judged by the invariant IR spectra, the sample was purged by N_2 at 350 °C till no changes happen to the IR spectra with the increasing time. The sample cell was subsequently heated to 500 °C at 10 °C/min, and NO_x desorption behaviors were recorded. The gas flow rate in all circumstances was 200 ml/min, and the tiny IR interference from gas molecules was subtracted.

In NSR activity tests, 0.5 g catalyst (0.2 g of 2 wt.% Pt/Al_2O_3) was mixed with quartz sand in a volume ratio of 1:3. The total flow rate is 1 L/min, with the space velocity of 30,000 h^{-1}. A NICOLET 380 FT-IR equipped with a 2-m gas cell was used to detect the outlet concentrations of NO, NO_2, NH_3, N_2O, CO, CO_2, and H_2O (g) at 4 s intervals. IR spectra of the multiple gases were collected at the same time. These spectra were automatically quantified by comparing them with the standardized spectra of diluted monocomponent gases at different concentrations, which were already set into mathematical functions as a method file. Home-developed software, OMINIC, TQ Analyst, and Macros Basic were connected to effectuate the calculations. A set of 1 min (lean)–1 min (rich) experiments and another set of 10 min (lean)–1 min (rich) experiments were conducted. The inlet gas concentrations are listed in Table 2. Calculations were made based on the reproducible concentration curves for at least 3 cycles (usually 5–6 cycles were required before stabilization). NO_x-TPD experiments were conducted on the same equipment with the same flow rate. Powder samples were pre-treated in 7.5% O_2/N_2 at 500 °C for 20 min, and

Table 2
Inlet gas concentrations of 1 min (lean)–1 min (rich) NSR tests.

Gases	Concentrations (by volume[a])	
	Lean periods	Rich periods
NO	500 ppm	500 ppm
O_2	7.5%	0
CO	0	7.5%
CO_2	10%	10%
H_2O	10%	10%
N_2	Balance	Balance

[a] NO injection was switched off in rich period of 10 min (lean)–1 min (rich) tests.

then cooled to 50 °C under N_2 protection. The catalysts were saturated in 1.68% NO/7.5% O_2/N_2. After N_2 purge, the samples were heated to 500 °C in N_2 at 10 °C/min. NO and NO_2 were the only components detected by MCT detector and were having similar product distributions with the temperatures due to the same Pt/Al_2O_3 part.

3. Results

3.1. Chemical and physical evolutions during aging

The effect of 10% CO_2 hydrothermal 12 h aging was first investigated over the 30 wt.% Ba-supported samples. The *ex situ* XRD patterns are shown in Fig. 1. Under this aging atmosphere, the formation of $BaCeO_3$ was not detected in either the 30 wt.% BaO/CeO_2 series (Fig. 1B) or the corresponding Pt-loaded samples (Fig. 1A). Peaks attributed to orthorhombic $BaCO_3$ ($BaCO_3$–O) and CeO_2 grew sharper after aging, indicating larger crystallites were formed due to particle sintering during the aging. Pt particles (not detected by XRD because of the high dispersion or low loading ratio) in proximity to the barium species and the ceria did not stimulate $BaCeO_3$ formation. Only the crystal sizes of the particles were modified by Pt impregnation, because the $BaCO_3$ can be dissolved by $Pt(NO_3)_2$ solution [20]. On the other hand, crystal decomposition of $BaCO_3$–O occurred in the cases of Ba/Al (Fig. 1C) and Ba/Zr (Fig. 1D) series. This phenomenon was accompanied by the appearance of $BaAl_2O_4$ and $BaZrO_3$, which were also detected in the Pt-loaded samples by other researchers [12,13]. Ceria materials resistance to the formation of $BaCeO_3$, regardless of the NM locations, provides an advantage over the other two support oxides. The following work is going to focus on the specific effects of CO_2 and H_2O during the aging treatments to Ba/Ce materials.

First, the capabilities of $BaCeO_3$ formation and decomposition were confirmed. The process of $BaCeO_3$ formation in BaCe11 during 0–18 h thermal aging in air and the regeneration of the 12 h thermal-aged sample in CO_2 are depicted by *in situ* XRD patterns in Fig. 2. After 12 h thermal aging, a significant amount of $BaCeO_3$ phase formed. This increasing trend continued through the thermal aging. In contrast, when a 10% CO_2 hydrothermal aging feed was introduced into the *in situ* reactor after 12 h thermal aging, the

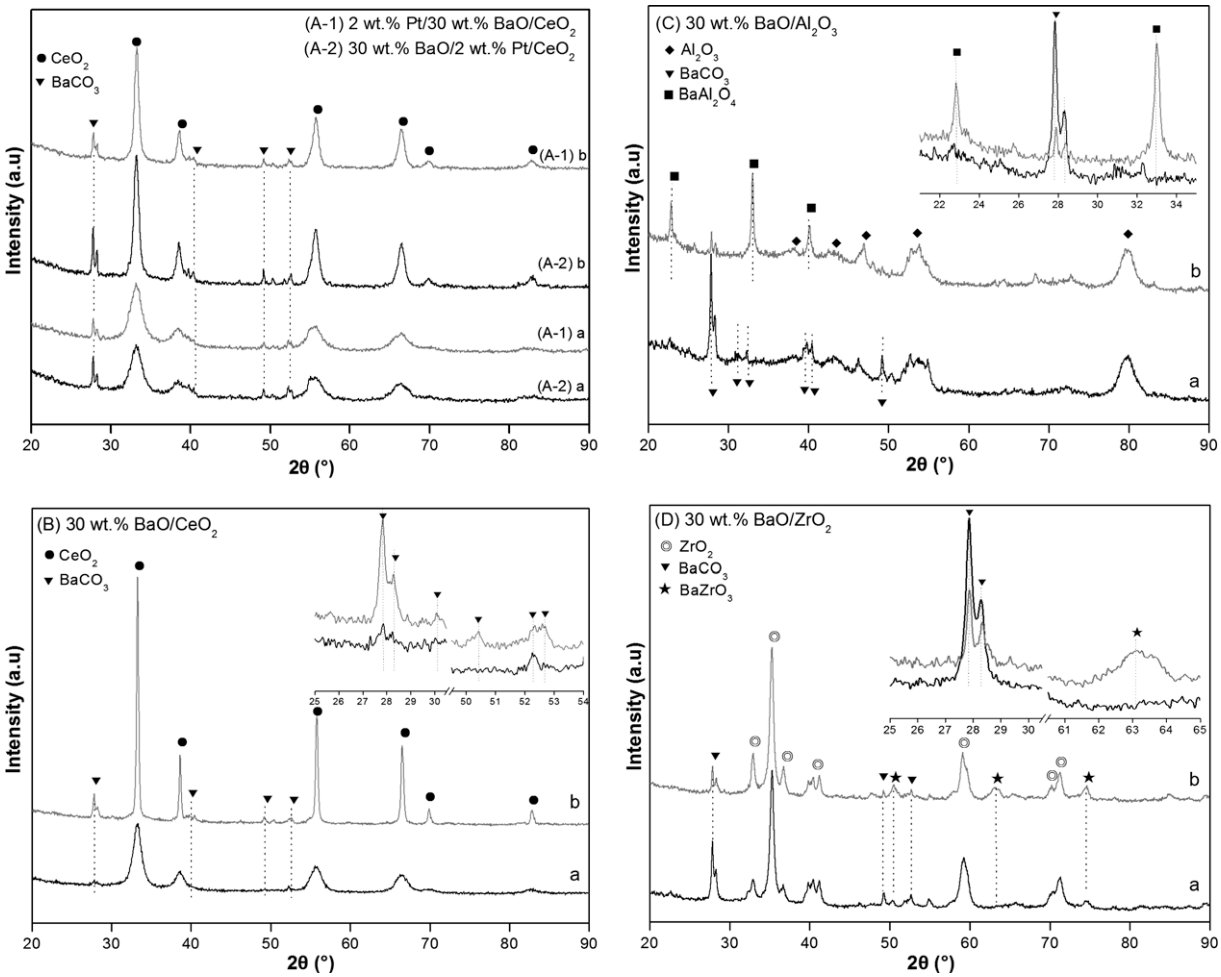

Fig. 1. XRD patterns of (a) fresh and (b) 10% CO_2 hydrothermal-aged samples with variant Pt loadings (A) or different support oxides (B–D). Part figures illustrate the major changes of crystallites between fresh (black) and aged (gray) samples in larger scales.

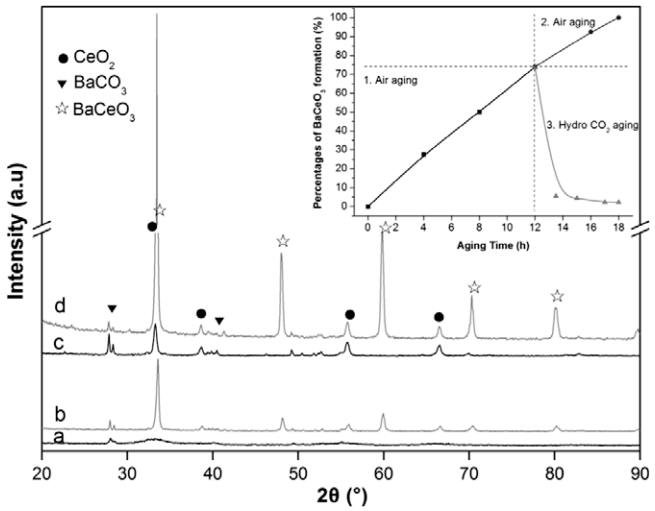

Fig. 2. *In situ* XRD patterns of (a) fresh, (b) 12 h thermal aged, (c) 6 h 10% CO_2 hydrothermal aged in addition to (b), and (d) 18 h thermal-aged BaCe11 compounds. Insert illustrates the progress in $BaCeO_3$ crystallization and decomposition (set the $BaCeO_3$ content in 18 h thermal-aged sample as 100%).

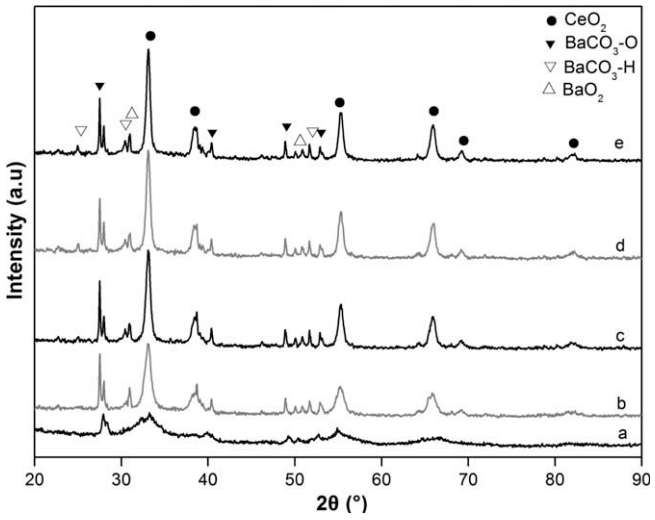

Fig. 3. *In situ* XRD patterns of BaCe11 compounds in their (a) fresh state (as-prepared sample at RT) and aged in 5% CO_2 thermal condition for (b) 0 h (as-prepared sample just reaching 800 °C), (c) 4 h, (d) 8 h, and (e) 12 h.

XRD peaks attributed to $BaCeO_3$ disappeared and the peaks attributed to CeO_2 and $BaCO_3$ re-appeared, indicating that the regeneration of $BaCeO_3$ to $BaCO_3$–O and CeO_2 crystallites occurred. The percentage of $BaCeO_3$ crystal formation (normalized to the crystal phase after 18 h thermal aging) was estimated based on the intensity of the diffraction features and is shown in the insert of Fig. 2. Although the existence of amorphous particles cannot be discounted [12], the overall trend clearly demonstrates the poor chemical stability of $BaCeO_3$ in 10% CO_2 hydrothermal conditions. The reappearance of $BaCO_3$–O and CeO_2 phases suggests that the balance between barium species and ceria has been shifted, and the formation of $BaCO_3$ and CeO_2 phases is favored over the formation of $BaCeO_3$ in the presence of 10% CO_2 and steam at 800 °C.

Second, the specific effects of CO_2 and steam in lean aging were studied separately. Fig. 3 presents the *in situ* XRD patterns for BaCe11 aged in a 5% CO_2 thermal condition. The results indicate that a CO_2 concentration as low as 5% is enough to suppress $BaCeO_3$ formation at 800 °C. Two new phases, hexagonal $BaCO_3$ ($BaCO_3$–H) and BaO_2, were detected. During the decarbonation, the phase transition of $BaCO_3$–O to $BaCO_3$–H occurs first [21]. Theoretical energy for the transformation from $BaCO_3$–O ($5.4 \times 9.0 \times 6.6$ Å^3, whiterite structure) to $BaCO_3$–H ($5.4 \times 5.4 \times 18.8$ Å^3, calcite structure) was estimated to be about 0.6 eV [22]. Hexagonal $BaCO_3$ has an intermediate stability and is of relevance to the start of NO_x trapping [22]. Previous studies [23,24] have addressed the positive role of BaO_2 as a metastable species during LNT, where O_2^{2-} can be stabilized in BaO_2 lattice under oxidative atmosphere and at higher temperatures [23]. These phases are believed to be active but very unstable. They were not detected at *ex situ* RT and *in situ* conditions without CO_2 or with steam (discussed later). The presence of 5% CO_2 promotes the stability of barium carbonates during the polymorphic transformations and inhibits the migration of decomposed Ba^{2+} and O^{2-} to the ceria lattice to form $BaCeO_3$. When using 10% CO_2 thermal *in situ*-aged samples, similar results can be found with only minor differences in barium species distributions (summarized in Table 3).

TG-DSC results (Fig. 4) record several stages of decompositions and solid reactions under different atmospheres. Weight loss below 300 °C is related to the decomposition of amorphous carbonates, and the weight loss over 600 °C is attributed to the decomposition of bulk structured carbonates [12,18,19]. The samples heated in air showed drastic weight loss right above 750 °C (A and B). Whereas the samples heated in 5% CO_2 showed continuous slight weight loss without drastic drops until 1000 °C (C and D). In accordance with the theoretical analysis [25], 100% decomposition of $BaCO_3$ above 1100 °C is thermodynamically inevitable in all the conditions we investigated. However, based on the DSC curves, we still notice that the decomposition of $BaCO_3$ in air only conditions is apparently more endothermic than that in air + CO_2 conditions. Since $BaCeO_3$ formation at 800 °C has been well documented [11,12], it is safe to conclude that the rapid weight loss at 800 °C, accompanied with the more endothermic peaks, is caused by the decomposition of carbonates and the simultaneous promoted $BaCeO_3$ formation. Anyway, it is not guaranteed that all the $BaCO_3$ decomposed can form $BaCeO_3$ with CeO_2 within the limited time span in one TG experiment. The presence of 5% CO_2 suppresses the $BaCeO_3$ formation promoted decomposition of $BaCO_3$ around 800 °C. This phenomenon is clearer in BaCe11 samples at all heating rates (results not shown for 5 and 15 °C/min tests), where the two temperature regions of decompositions can be well defined

Table 3
Percentages of detected Ba-based crystallites and particle sizes calculated based on *in situ* XRD patterns of BaCe11 compounds after 12 h aging treatments.

Aging treatments	Percentages of detected Ba-based crystallites (%) (experimental error 5%)				$BaCeO_3$ particle sizes (Å)	Orthorhombic $BaCO_3$ particle sizes (Å)
	BaO_2	Hexagonal $BaCO_3$	Orthorhombic $BaCO_3$	$BaCeO_3$		
Thermal	–	–	21	44	250 ± 15	na
Hydrothermal	–	–	5	72	352 ± 11	na
5% CO_2 thermal	14	16	25	–	–	106 ± 11
10% CO_2 thermal	14	14	30	–	–	117 ± 11
5% CO_2 hydrothermal	–	–	60	–	–	150 ± 15
10% CO_2 hydrothermal	–	–	76	–	–	190 ± 45

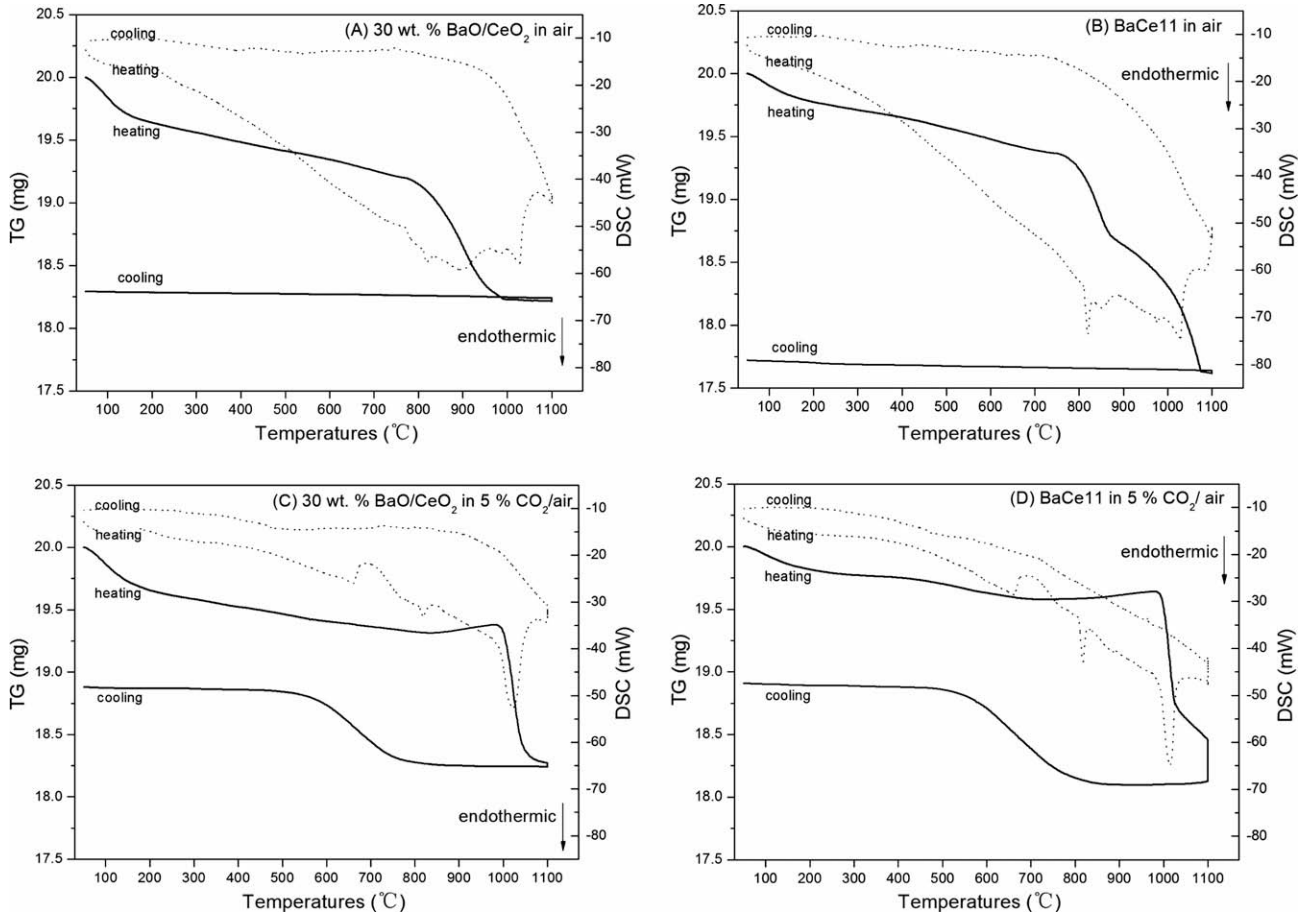

Fig. 4. TG (black) and DSC (gray dashed) curves of the samples heated from 50 to 1100 °C at the rate of 10 °C/min, stabilized at 1100 °C for 20 min, and cooled back at the rate of −10 °C/min in air (A and B) air, and 5% CO_2/air (C and D).

with the narrow endothermic DSC peaks located at 800 (minor) and 1000 °C (major), corresponding to the idealized pure decarbonation process [25], and the interference of CeO_2 support oxide should be very limited even at 1100 °C due to the barrier for $BaCeO_3$ formation. According to the method proposed by Tomashevitch et al. [26], we assume a kinetics equation for the decomposition reaction:

$$\frac{\partial\alpha}{\partial\tau} = k_0 \exp\left(-\frac{E_A}{RT}\right) f(\alpha) \tag{1}$$

α is the degree of conversion, k_0 the pre-exponential factor, E_A the activation energy, and $f(\alpha)$ the temperature independent kinetic function. At high temperatures, the reciprocal temperature growth is almost a linear function of time (Fig. 5):

$$\frac{1}{T(\tau)} = \frac{1}{T_0} + \gamma T \tag{2}$$

Eq. (1) can thus be integrated, and the activation energy E_A can be obtained from at least two experiments with different γ_i, without any assumptions of functional form of $f(\alpha)$:

$$\frac{1}{\gamma_5}\left\{1 - \exp\left(-\frac{E_A\gamma_5\tau}{R}\right)\right\} = \frac{1}{\gamma_{10}}\left\{-\exp\left(-\frac{E_A\gamma_{10}\tau}{R}\right)\right\} = \frac{1}{\gamma_{15}}\left\{1 - \exp\left(-\frac{E_A\gamma_{15}\tau}{R}\right)\right\} \tag{3}$$

It is observed that in air flow, the activation energy of $BaCO_3$ decomposition is 145 ± 25 kJ/mol around 800 °C (promoted by ceria contact) and 250 ± 17 kJ/mol above 1000 °C. Whereas the E_A is as high as 500 ± 17 kJ/mol for CO_2 protected samples throughout the heating process. This is similar with the theoretical calculation results [27], predicting an almost one time higher E_A is required for $BaCO_3$ decomposition in CO_2 contained flows, invariant with CO_2 partial pressures. When the temperatures were decreased to 800 °C from 1100 °C, the regaining of weight happened on the samples treated in 5% CO_2/air flow, indicating the chemical balance is moving toward the carbonates formation again.

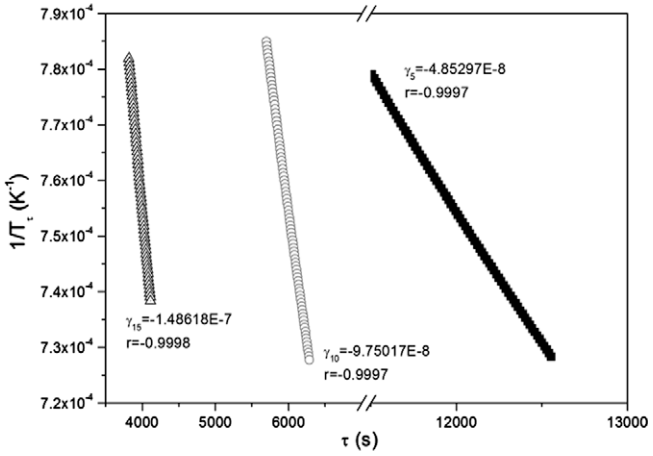

Fig. 5. Reciprocal heating rate constants γ_5, γ_{10}, and γ_{15} corresponding to the heating rates of 5, 10, and 15 °C/min, respectively. When the percentages of $BaCO_3$ decomposition (α) are in the range of 20–90%, reaction time (τ) was big enough to guarantee the hyperbolic temperature–time curves be fitted in linear way.

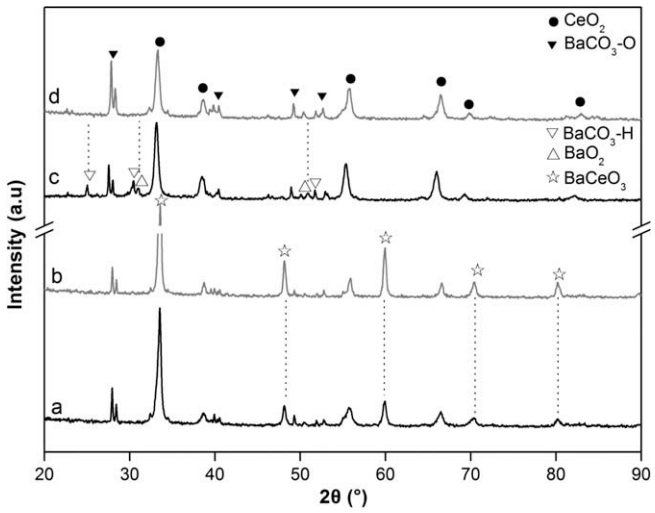

Fig. 6. *In situ* XRD patterns of BaCe11 compounds treated for 12 h in (a) thermal, (b) hydrothermal, (c) 10% CO_2 thermal, and (d) 10% CO_2 hydrothermal conditions.

The effects of steam are more morphological than chemical. For the *in situ* XRD patterns in Fig. 6, the difference mainly involves the crystallinity of different compositions, and the overall chemical equilibrium between barium species and ceria species is still dominated by CO_2. In the cases of thermal aging and hydrothermal aging, $BaCeO_3$ was detected. In the presence of 10% steam, changes in crystallites are more pronounced than the thermally aged sample. A more noticeable increase in $BaCeO_3$ crystallinity is accompanied by a significant decrease in CeO_2 and $BaCO_3$–O XRD peaks. However, this does not necessarily imply that steam inhibits the stabilization carbonates in the presence of CO_2. During the aging processes when 10% CO_2 was present, the formation of $BaCeO_3$ was absent regardless of the presence of steam. For the 10% CO_2 hydrothermal-aged sample (Fig. 6d), the crystallite growth of $BaCO_3$–O is higher than that of the 10% CO_2 thermal-aged sample (Fig. 6c). Furthermore, *in situ* XRD patterns in Fig. 6d show no evidence of BaO_2 and $BaCO_3$–H crystal's existence. Therefore, regardless of CO_2 existence, steam in the aging atmosphere seems to serve only as a promoter for the crystal growth of the most stable ceria and barium phases in certain aging conditions.

The percentages of crystalline barium phases [12] and their crystal sizes are calculated based on XRD patterns (Table 3). The particle sizes of $BaCO_3$–H and BaO_2 are unable to be calculated because of their scattered weak peaks. In sum, $BaCO_3$, BaO_2, CeO_2, $BaCeO_3$ can coexist in aging conditions. Under the protection of CO_2, orthorhombic $BaCO_3$ and CeO_2 are the most stable components below 800 °C. Steam accelerates the morphological changes, but it does not determine the above chemical equilibrium. Larger crystal sizes of the thermodynamic favored stable phases can be detected in the presence of steam and higher concentrations of CO_2.

The changes of surface areas during the aging are listed in Table 4. For both BaCe11 and 30 wt.% BaO/CeO_2 samples, the trends of the surface areas' changes are similar. In the absence of CO_2, more significant decrease in surface areas is observed. Although the decomposition of barium carbonates before the formation of $BaCeO_3$ crystallites may contribute to the increase in surface area [28], this effect was not observable here. The surface areas of the samples aged in CO_2 are generally higher, especially for those samples aged in lower concentrations of CO_2. The presence of steam in the aging atmosphere results in lower surface areas. In comparison with BaCe11 compounds, 30 wt.% BaO/CeO_2 samples with higher initial surface areas suffered the more obvious surface areas declines after aging. Because of the significant sintering effect, even with similar distribution of chemical components, the catalytic activity of 30 wt.% BaO/CeO_2 inevitably decreases along the increasing aging times (activity data not shown for brevity). SEM images of 30 wt.% BaO/CeO_2 samples illustrated in Fig. 7 further confirm the influences of different aging conditions. In the absence of CO_2, formation of $BaCeO_3$ (light color) in downy shape takes place, and the spherical structures of 30 wt.% BaO/CeO_2 are destroyed severely. The presence of CO_2 not only suppresses $BaCeO_3$ formation, but also manages to maintain the original morphologies of the catalysts to some extent. Among all the cases we investigated, the introduction of water promotes the aggregation of the particles.

Table 4
Surface areas of BaCe11 and 30 wt.% BaO/CeO_2 after 12 h different aging treatments.

Aging treatments	S_{BET}[a] (m^2/g) and decreasing percentages			
	BaCe11		30 wt.% BaO/CeO_2	
Thermal	9.7	50.5%	18.7	77.4%
Hydrothermal	7.9	59.7%	10.0	88.0%
5% CO_2 thermal	11.4	41.8%	31.8	61.6%
10% CO_2 thermal	10.7	45.4%	31.1	62.5%
5% CO_2 hydrothermal	10.7	45.4%	23.9	71.2%
10% CO_2 hydrothermal	10.8	44.9%	22.4	73.0%

[a] S_{BET} of the fresh BaCe11 and 30 wt.% BaO/CeO_2 are 19.6 and 83.0 m^2/g, respectively.

3.2. Catalytic activity changes induced by aging

Different aging treatments have brought about significant influences on NO_x adsorption and desorption behaviors in NSR reactions. Referred to the recent literatures [29–31], specific assignments of the IR bands are labeled in Figs. 8 and 9. The designations Al, Ce, and Ba suggest the surfaces where adsorbates are bonded. During NO_x adsorption (Fig. 8), bands attributed to bridged nitrate on Al_2O_3 were found around 1240 cm^{-1}, chelating nitrate on Al_2O_3 at 1570 cm^{-1}, nitrate on CeO_2 at 1535 cm^{-1}, $NO_2^{\delta+}$ on CeO_2 around 1780–1760 cm^{-1}, monodentate nitrate associated with BaO around 1291 cm^{-1}, and ionic nitrate associated with BaO around 1360–1350 cm^{-1}. The order of these bands introduced is in line with their stability from low to high. The major bands of ionic nitrate associated with BaO and minor bands of nitrate on CeO_2 were able to be maintained after N_2 purge (Fig. 9). Formation of nitrite was not detected in the experiments because of the high reaction temperature, and the pre-adsorption of water and oxygen on catalysts' surface during aging can be excluded by the pre-treatment.

After mixing 30 wt.% BaO/CeO_2 with 2 wt.% Pt/Al_2O_3, the adsorption behaviors of the catalysts are very different from pure 2 wt.% Pt/Al_2O_3 (almost no adsorption after N_2 purge), indicating the main storage function of BaO/CeO_2 part. The bands of ionic nitrate appear after the evolution of other increasing nitrate bands. The maintenance of these bands after N_2 purge (Fig. 9) indicates their higher stability, and the stabilization of these nitrate species should be closely related to the activity on the major NO_x storage sites [29]. Adsorptions over fresh catalyst show the highest IR intensity, whereas the samples with increasing amount of $BaCeO_3$ formation or/and higher level of crystallinity (either $BaCeO_3$ or $BaCO_3$) suffered the decrease in adsorption intensity, especially on barium and ceria sites The deactivations of BaO/CeO_2 parts during aging are not only indicated by the weaker IR intensity, but the distributions of their IR signals appear to be more similar to those of Pt/Al_2O_3. Fine active phases, including $BaCO_3$–O, $BaCO_3$–H, and BaO_2 which are inclined to be maintained in CO_2, are believed to benefit the NO_x storage amount and rate and to facilitate the major trapping capacity on BaO/CeO_2.

At the beginning of the desorption, little evidence of nitrate/nitrite adsorption can be observed on 2 wt.% Pt/Al_2O_3 sample (Fig. 9),

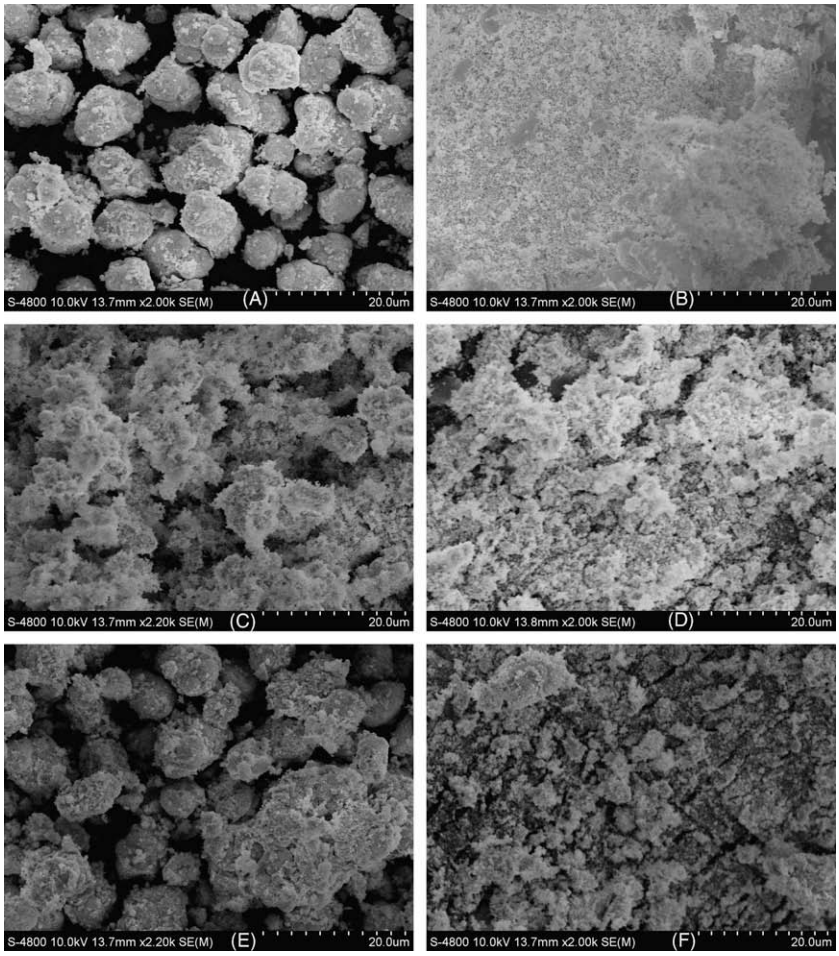

Fig. 7. SEM images of 30 wt.% BaO/CeO_2 in (A) fresh state, and treated in (B) 1100 °C calcinations in air for 4 h, (C) thermal, (D) hydrothermal, (E) 10% CO_2 thermal, and (F) 10% CO_2 hydrothermal aging conditions.

indicating the negligible stable NO_x storage capacity of Pt/Al_2O_3 at 350 °C. Moreover, the initial difference among the other five spectra (NO_x saturated) at 350 °C is not as significant as that in the previous adsorption measurements with time limit, indicating the increasing crystallinity or/and $BaCeO_3$ formation not only decreases the amount of active sites, but can hinder the NO_x trapping rate. For thermal and hydrothermal-aged samples, limited amount of nitrate bonds dissociated below 400–450 °C, but the NO_x desorption is greatly accelerated right above 450 °C. In contrast, IR bands of nitrate over fresh and CO_2-aged samples decreases in a milder manner with the increasing temperatures, and higher amount of surface nitrate adsorbates has been released in every temperature range. Monodentate nitrate, having lower thermal stability than ionic nitrate, reappears above 400 °C. These stabilizing effects to metastable adsorbates remind us the above *in situ* XRD observations of multiple $BaCO_3$ phases and BaO_2 in CO_2 without steam. In the N_2 flow, the existence of metastable phases and oxidative sites provides intermediate nitrate species a higher possibility to be stabilized on catalysts' surface.

NO_x-TPD result (Fig. 10) also shows that Pt/Al_2O_3 has limited NO_x trapping capability, when compared with that of BaO/CeO_2 part. The saturated amount of adsorbed NO_x of the aged samples is obviously different. But it is not as significant as that in the *in situ* adsorption process with time limit, in which the trapping rates are going to make larger differences. As revealed by the data, $BaCeO_3$ formation still weighs the worst for NO_x trapping, and the higher crystallinity of $BaCO_3$ induced by coexistence of steam and CO_2 shows minor negative role for the overall NO_x trapping capacity. As the DRIFTS results indicated, NO_x adsorption on Ce sites has very poor stability under N_2 purge at 350 °C. Therefore, NO_x sorption on active ceria sites can only contribute to low temperature adsorptions, and the NO_x desorption peaks above 350 °C should be mainly related to the activity of barium sites, pertaining to barium nitrate decomposition. In accordance with the DRIFTS results (Fig. 9), the thermal and hydrothermal-aged samples not only show the weakest desorption intensity, but their desorption processes quickly completed around 400–450 °C. For the CO_2-aged samples, neither $BaCeO_3$ formation nor the most severe sintering happens, and the NO_x desorption above 400 °C is still noticeable and is only less than that of the fresh catalyst. The higher crystallinity of carbonates and the aggregation of support oxides, especially when steam and CO_2 exist, are the contributing factors for the decline.

Catalytic performances of 2 wt.% Pt/Al_2O_3 + 30 wt.% BaO/CeO_2 catalysts were evaluated at 350 °C, where the NO oxidation over Pt/Al_2O_3 is not the rate controlling step, and the aging effects on barium species should be more obvious. Exposure in a lean period for 10 min is sufficient for the samples to approach the NO_x saturated stage. Table 5 lists the key data of the evaluations. Samples containing $BaCeO_3$ (after thermal and hydrothermal aging treatments) suffered the greatest activity decrease in comparison with the fresh catalyst. To another extreme, without $BaCeO_3$ formation, samples aged under high concentrations of CO_2 and steam also suffered an obvious but minor decrease in NSC. During the rich period, NO was switched off, and only the NO_x released from the storage sites participated in the reduction process. It is observed that

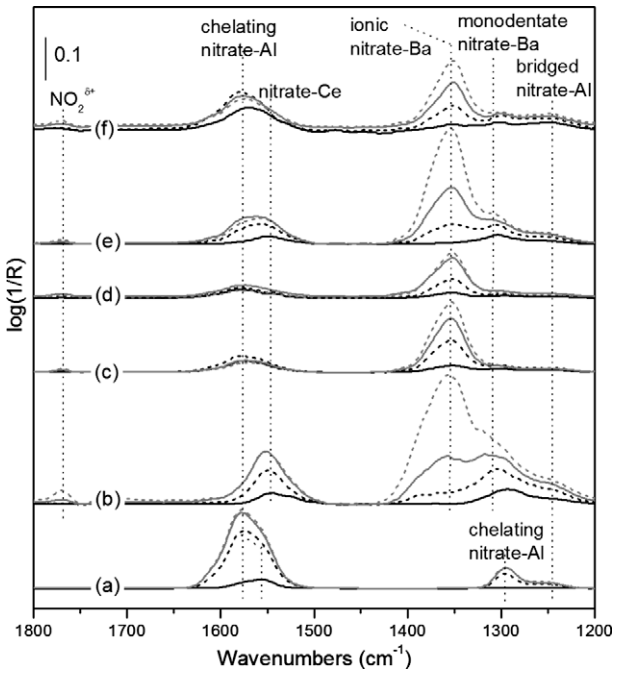

Fig. 8. *In situ* DRIFTS spectra recorded at 5 (black), 10 (black dashed), 15 (gray), and 20 (gray dashed) min during NO_x adsorption at 350 °C on (a) 2 wt.% Pt/Al_2O_3, and 2 wt.% Pt/Al_2O_3 + 30 wt.% BaO/CeO_2 catalysts in (b) fresh, (c) thermal, (d) hydrothermal, (e) 10% CO_2 thermal aged, (f) 10% CO_2 hydrothermal states.

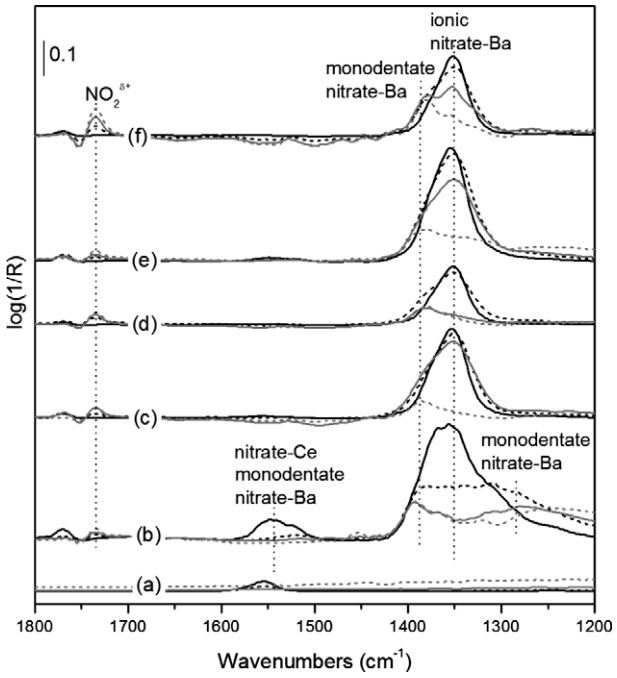

Fig. 9. *In situ* DRIFTS spectra recorded at 350 (black), 400 (black dashed), 450 (gray), and 500 (gray dashed) °C during NO_x adsorption from 350 to 500 °C at the heating rate of 10 °C/min on (a) 2 wt.% Pt/Al_2O_3, and 2 wt.% Pt/Al_2O_3 + 30 wt.% BaO/CeO_2 catalysts in (b) fresh, (c) thermal, (d) hydrothermal, (e) 10% CO_2 thermal aged, (f) 10% CO_2 hydrothermal states.

catalysts with a higher NSC generally release a higher amount of NH_3 and a lower fraction of unreduced NO during the rich periods, compared with the amount of NO_x trapped during the lean periods. Reducing agent should be excessive in such a case, and higher crystallinity of the materials after aging inhibits the efficient NO_x release and reduction.

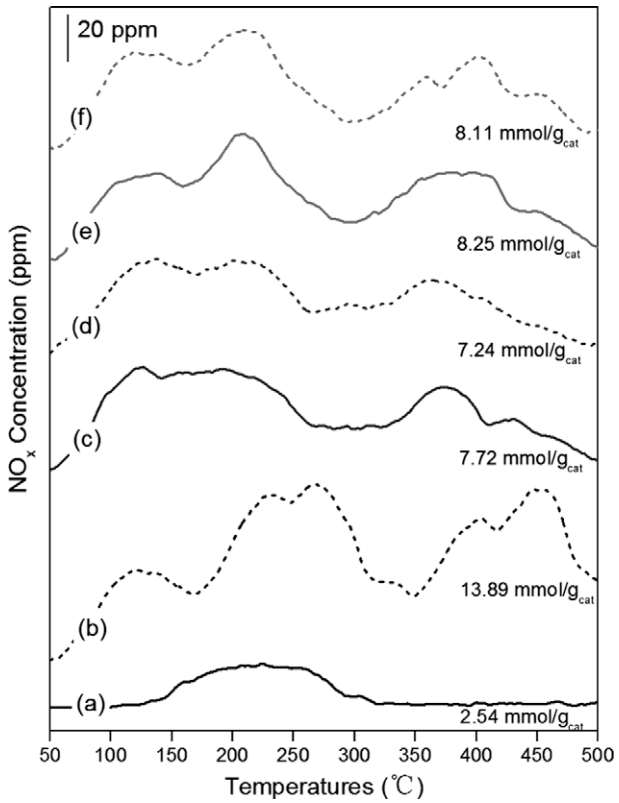

Fig. 10. NO_x-TPD profiles of (a) 2 wt.% Pt/Al_2O_3 (0.2 g), and 2 wt.% Pt/Al_2O_3 (0.2 g) + 30 wt.% BaO/CeO_2 (0.3 g) catalysts in (b) fresh, (c) thermal, (d) hydrothermal, (e) 10% CO_2 thermal aged, (f) 10% CO_2 hydrothermal states. Total amount of NO_x desorbed is labeled beside the curves.

Another set of tests was conducted in 1 min–1 min lean–rich cycles with non-stopping NO injections during rich periods. Fig. 11 illustrates the periodic evolution of NO, NO_2, N_2O, NH_3, CO, CO_2, and H_2O concentrations. H_2 and CO coexisted during the rich periods because of the WGS reaction. The NH_3 "tail" was observed at the beginning of lean period. Because NH_3 is a "sticky" gas in the reactor sampling lines, the lag from the NH_3 signal in the FT-IR analysis becomes possible [32]. Besides the NO breakthrough during the rich periods, N_2O release was also detected, but it became less noticeable when the temperature increased.

Not only the formation of sintered $BaCeO_3$ does, but the increased crystallinity of carbonates has a negative effect on the rapid storage and complete release of NO_x. The concentrations of NO, NO_2, and NH_3 at 350 °C are shown in Fig. 12. The amount of NO_x stored during the 1 min lean period was compared with the saturated amount of NO_x after 10 min (Table 5). The aged samples without the formation of $BaCeO_3$ show higher NO_x trapping capacities and rates. But if the samples were aged in higher concentrations of CO_2 and steam, their advantages have been weakened. For the samples that show higher NSC during the lean periods, the corresponding amounts of NO_x and NH_3 released during the rich periods are less. The NH_3 formed in the forefront of catalysts' bed during rich conditions can further react with the injected and released NO through the catalysts, especially when residual oxygen in gas phase or ceria lattice oxygen can participate in the favorable NH_3–NO–O_2 reduction [33–35]. Due to the oxygen storage capacity (OSC) of CeO_2, the ceria lattice may supply oxygen to participate in the NO_x reduction [36]. To further confirm this, we used 4% CO/N_2 and 2% O_2/N_2 as the 1 min rich and lean atmospheres, respectively, between which a 1 min N_2 purge was applied. The OSC activity was evaluated based on the amount of CO_2 produced in rich periods (Table 5). The CO_2 production of all samples in lean periods is

Table 5
Performances of the 2 wt.% Pt/Al_2O_3 + 30 wt.% BaO/CeO_2 catalysts prepared using different aging treatments during 10 min (lean)–1 min (rich) NSR cycles at 350 °C.

Samples	Lean NO_x stored ($\mu mol/g_{cat}$) and percentages of NO_x stored in 1 min		Rich NH_3 released ($\mu mol/g_{cat}$) and percentages to NO_x stored in 10 min		Rich NO_x released ($\mu mol/g_{cat}$) and percentages to NO_x stored in 10 min		OSC in 1 min rich period ($\mu mol/g_{cat}$)
Fresh	67.0	99.9%	36.2	54.0%	5.6	8.4%	213.6
Thermal	46.1	87.0%	35.0	75.9%	8.9	21.8%	167.9
Hydrothermal	40.9	78.0%	27.3	66.7%	10.7	23.2%	156.7
5% CO_2 thermal	60.3	82.9%	39.0	64.7%	5.3	8.8%	195.8
10% CO_2 thermal	58.8	78.0%	35.8	61.0%	7.1	12.1%	195.0
5% CO_2 hydrothermal	56.5	78.2%	32.1	56.7%	8.7	15.4%	189.2
10% CO_2 hydrothermal	55.8	78.3%	28.3	50.7%	9.2	16.5%	186.1

* The 1 min NSCs for 2 wt.% Pt/30 wt.% BaO/CeO_2 samples are 103.0 $\mu mol/g_{cat}$ (fresh) and 87.5 $\mu mol/g_{cat}$ (10% CO_2 hydrothermal).
* The 1 min NSCs for 30 wt.% BaO/2 wt.% Pt/CeO_2 samples are 94.7 $\mu mol/g_{cat}$ (fresh) and 78.3 $\mu mol/g_{cat}$ (10% CO_2 hydrothermal).
* The 1 min NSC for fresh 2 wt.% Pt/Al_2O_3 is 14.6 $\mu mol/g_{cat}$.

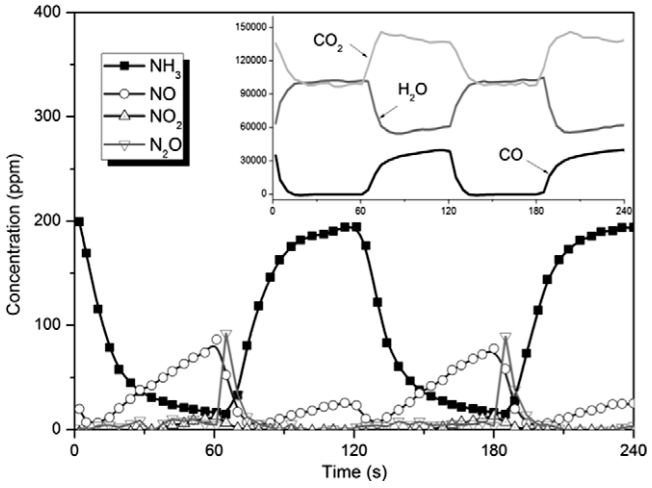

Fig. 11. 1 min (lean)–1 min (rich) NSR reaction profiles of NH_3, NO, NO_2, and N_2O at 300 °C. Insert illustrates the periodic changes of CO, CO_2, and steam concentrations.

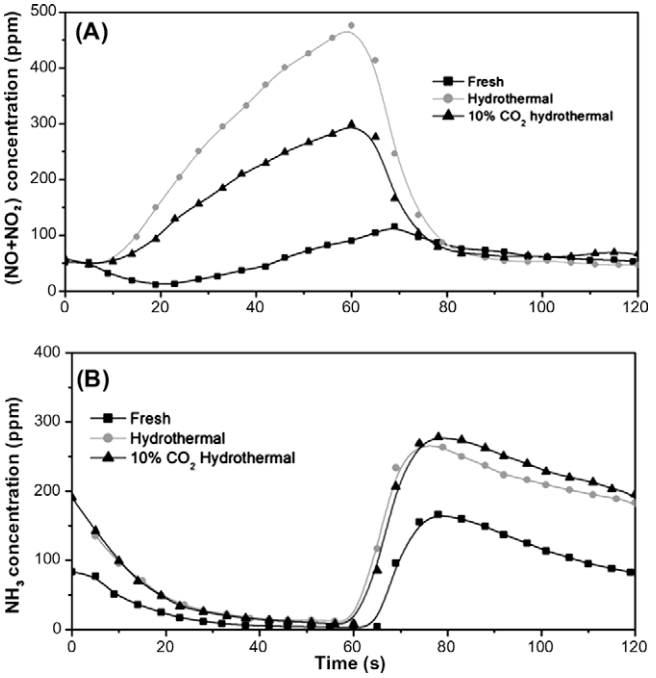

Fig. 12. NSR response curves at 350 °C for (A) NO + NO_2 and (B) NH_3 during a complete lean–rich cycle with different 2 wt.% Pt/Al_2O_3 + 30 wt.% BaO/CeO_2 catalysts.

around 90–100 $\mu mol/g_{cat}$, which is related to the similar CO adsorptions in the previous rich period [37]. Generally, ceria-based catalysts that suffer less extent of thermal deterioration produce higher amount of OSC in rich conditions, and the trace amount of oxygen species released from ceria seems to have positive correlation with N_2 selectivity. However, we are reserved to claim that higher OSC should be desirable for lean NO_x storage. According to the concentration curves (Fig. 12), we observed that the NO_x concentration in lean period keeps going down for 50 ppm in 20 s for the fresh sample at 350 °C, but this did not happen for other aged samples with lower OSC. Since the same Pt/Al_2O_3 part for NO oxidation has been applied, the states of fresh ceria should be the main contributing factor here. It is inferred that this hindering effect of NO_x trapping at the very beginning of the lean period is due to the higher amount of Ce^{3+} formed and residual reducing agent adsorbed on ceria surface after the pervious rich period [37,38]. If the OSC activity is lower, which means the CeO_2 support oxides have less Ce^{3+} and be more oxidative, NO_x should be stored and stabilized more easily at the beginning of the lean period. In such a sense, higher OSC is not desirable in our specific conditions.

4. Discussion

4.1. Effect of CO_2 in lean aging

In terms of materials' activity, we find that, to some extent, the presence of CO_2 has a positive effect in maintaining the NO_x trapping sites in barium species. Without CO_2 during high temperature aging, $BaCO_3$ can easily decompose into BaO and form $BaCeO_3$ with CeO_2 at 800–850 °C. The solid reaction between the Ba–Ce phases on catalysts' interfaces diminishes large quantity of NO_x trapping sites for stable nitrate formation. Moreover, as the two phases almost crashed into the lattice of each other during $BaCeO_3$ formation, the accompanied severe sintering of the catalysts greatly decreases the nitrate' stability. Fortunately, as little as 5% CO_2 hinders the formation of $BaCeO_3$ to even 1000 °C hydrothermal aging and improve the overall performance. Since CO_2 is present in lean-burn exhaust with a normal concentration around 10%, the driving force of Ba/Ce catalysts' deactivation has been reconsidered in the present work. Low concentrations of CO_2 in aging atmosphere manage to maintain the chemical equilibrium among $BaCO_3$, BaO, BaO_2, $Ba(OH)_2$, and CeO_2. Because the thermodynamic equilibrium to $BaCeO_3$ formation is not favored in such circumstances, decarbonation of $BaCO_3$ particles in close contact with CeO_2 shows no significant difference to that of pure $BaCO_3$ [27]. The competition of CO_2 with NO_x for barium sites has been reported to be negative in NSR reactions [5,36]. However, when low concentrations of CO_2 in the exhaust manage to avoid $BaCeO_3$ formation, and to maintain the metastable phases ($BaCO_3$–H and BaO_2) as fine particles, the

abundant nitrate in stable bonding with barium surface and efficient diffusion in bulk structure are less hindered by the high temperature treatment. Therefore, their dynamic NSR activity becomes more desirable among the aged samples.

4.2. Effect of steam in lean aging

Steam promotes the crystal growth of stable phases in thermodynamics during the aging. The inferior NO_x storage and reduction efficiency on bulk structures of barium species have been documented in many works [16,35]. Water-induced morphological modifications over barium-based materials have been recently performed [39], and the effects of steam on the formation of bulk structured nitrate were corroborated. In our case, the effects of steam in lean aging mainly involve accelerating the aggregation of particles. In the absence of CO_2, the presence of steam further promotes both the crystallization of $BaCeO_3$ and the decomposition of $BaCO_3$. While with CO_2 to inhibit the formation of $BaCeO_3$, steam promotes the crystallization of $BaCO_3$–O, thus eliminating the intermediate phases such as $BaCO_3$–H and BaO_2. Whenever steam was present during the aging process, more severe sintering was observed. For NSR activities, concentration of steam shows a minor influence when compared with that of CO_2, because it does not stimulate any new deactivating chemical reactions during the aging. Formation of $BaCeO_3$ is more detrimental than the higher crystallinity to efficient NSR cycles.

4.3. Deterioration of Ba/Ce-based NSR catalysts in lean-burn condition

The presence of CO_2 and steam during lean aging treatments induces obvious morphological and chemical changes to the Ba/Ce-based NSR catalysts, and thus significantly modifies the catalytic performances. No matter if NM particles are in close contact with BaO/CeO_2 or not, the Ba-support interactions determine the composition and morphology of the barium components during the aging treatments. However, according to the NSR activity (fresh and aged) of 2 wt.% Pt/30 wt.% BaO/CeO_2 and 30 wt.% BaO/2 wt.% Pt/CeO_2 samples listed in Table 5, it is safe to conclude that the difference in percentile is weakened when fresh Pt is added directly to BaO/CeO_2 in our experimental conditions. Close Pt–Ba contact, which benefits NO_x spilling over to barium storage sites [14], is the main reason that increases the NSC of Pt added samples. On the other hand, for the samples with direct Pt–Ce contact, NO oxidation activity can be decreased to some extent, due to the surface basicity [40]. Moreover, the Pt particles fully oxidized by ceria lattice oxygen may gradually become deactivated for lean NO_x reduction and even oxidation [37,41]. In this sense, the addition of Pt makes the situation even complicated, especially when the aging treatments are going to significantly modify the morphologies and compositions of ceria-based components. Having very limited NO_x trapping capacity, fresh Pt/Al_2O_3 is applied in all the test conditions. By using such a catalyst' formulation, we expected to exclude the influence of different NO oxidation activity from Pt sites, and thus more precisely describe the changes and aging mechanisms in Ba–Ce interactions.

In the aging exhaust containing CO_2, the formation of $BaCeO_3$ is thermodynamically suppressed, and the activity decline due to the particle aggregations of BaO/CeO_2 materials needs more consideration. In order to obtain higher activity, NO_x, oxidized on the Pt sites, is expected to migrate quickly to the storage sites and transform into stable nitrate in lean conditions. In rich periods, the stored nitrate should be easily decomposed into NO_x for reduction. Being promoted by steam, higher concentrations of CO_2 break the equilibrium among $BaCO_3$–O, $BaCO_3$–H, and BaO_2. Not only is the formation of $BaCeO_3$, which consumes carbonates and induces severe sintering, being suppressed, but the aging causes more barium species to stabilize into bulk structured $BaCO_3$–O and sintered CeO_2. Larger barium particles create extra diffusion barriers for the formation/release of a large quantity of nitrite/nitrate in barium particles. Moreover, the stability of the weakly bonded nitrite and nitrate adsorbates can be drastically decreased by lowering the partial pressure of oxygen and favoring the exothermic reduction [42]. Because of the weak bonding with barium surfaces, nitrite/nitrate in larger barium particles rapidly decompose when encountering rich atmosphere or extra reaction heat. Much unreduced NO left the catalysts' bed in such conditions. Therefore, a decrease in NO_x reduction efficiency was observed, even though the total amount of trapped NO_x is less compared with the samples having better NSC. Milder NO_x release during the rich periods allows sufficient gas–solid contact for the released NO_x to be reduced into N_2 or NH_3 by Pt-catalysts. The NH_3 can then react with the NO in the adjacent zones of the catalyst bed to produce N_2 [34,35]. The formation of NH_3 is positively correlated with the efficient regeneration of NSC during the rich periods. A passive SCR catalyst following the NSR catalyst would be a beneficial utilization of the released NH_3. The lattice oxygen released by ceria may improve NO_x reduction by increasing N_2 selectivity [36,43]. But the higher Ce^{3+} content in reduced CeO_2 may destabilize the nitrate/nitrite formation on the catalysts surface at the beginning of the lean periods. OSC activity is in positive relationship with the less extent of sintering of CeO_2 support oxides, but it does not always guarantee the better NSR efficiencies. However, situations may be different when different lean–rich cycle lengths, gas concentrations, and ceria contents were applied [44,45].

5. Conclusions

Because CO_2 and steam are present in lean-burn exhaust with percentages of about 10% in volume, their effects on the morphological and chemical properties of Ba-based NSR catalysts during aging treatments should be noted. The formation of $BaAl_2O_4$ and $BaZrO_3$ over Ba/Al and Ba/Zr systems, respectively, can be detected after 800 °C 10% CO_2 hydrothermal aging for 12 h. However, in Ba/Ce-based catalysts, CO_2 concentration as low as 5% (air balanced) can sufficiently suppress the formation of $BaCeO_3$ or decompose the pre-existing $BaCeO_3$ easily. Active and metastable NO_x trap phases, such as hexagonal $BaCO_3$ and BaO_2, are able to be maintained because of the chemical equilibrium established by low concentrations of CO_2. During the decarbonation of $BaCO_3$ on CeO_2, CO_2 raises its activation energy to the level of pure $BaCO_3$ crystallites, and thus sets off the promoting effect of CeO_2 support oxide in accelerating the decarbonation by forming Ba–Ce compounds. However, when more CO_2 and steam are injected, the chemical equilibrium moves toward further stabilization of the storage components. Many original NO_x trapping phases in fresh samples transform into bulk structured $BaCO_3$ and CeO_2. The diffusion barriers for nitrate in bulk structure and the weak nitrite/nitrate bonding on catalysts' surface inhibit the efficient NO_x sorption and mild release. For Ba-based NSR catalysts developed for better performance after aging, the effects of CO_2 and steam in the aging atmosphere should be thoroughly considered since they are key agents in modifying the morphology and chemistry of the catalysts.

Acknowledgments

The authors are grateful to the financial support from the Program of New Century Excellent Talents in University (NCET-06-0243), the National 863 Program (No. 2009AA064803), the Program of Natural Science Foundation of China (No. 50972104), and the Key Program of Tianjin Natural Science Foundation (No. 09JCZDJC26600).

References

[1] N. Takahashi, H. Shinjoh, T. Iijima, T. Suzuki, K. Yamazaki, K. Yokota, H. Suzuki, N. Miyoshi, S. Matsumoto, T. Tanizawa, T. Tanaka, S. Tateishi, K. Kasahara, Catal. Today 27 (1996) 63.
[2] W.S. Epling, L.E. Campbell, A. Yezerets, N.W. Currier, J.E. Parks II, Catal. Rev. 46 (2004) 163.
[3] S. Roy, A. Baiker, Chem. Rev. 109 (2009) 4054.
[4] J. Kašpar, P. Fornasiero, M. Graziani, Catal. Today 50 (1999) 285.
[5] E.C. Corbos, X. Courtois, N. Bion, P. Marecot, D. Duprez, Appl. Catal. B: Environ. 76 (2007) 357.
[6] M. Fernández-García, A. Iglesias-Juez, A. Martínez-Arias, A.B. Hungría, J.A. Anderson, J.C. Conesa, J. Soria, J. Catal. 221 (2004) 594.
[7] E. Aneggi, M. Boaro, C. de Leitenburg, G. Dolcetti, A. Trovarelli, J. Alloy Compd. 408 (2006) 1096.
[8] H.Y. Lin, C.J. Wu, Y.W. Chen, C.H. Lee, Ind. Eng. Chem. Res. 45 (2006) 134.
[9] R. Strobel, L. Mädler, M. Piacentini, M. Maciejewski, A. Baiker, S.E. Pratsinis, Chem. Mater. 18 (2006) 2532.
[10] R. Strobel, F. Krumeich, S.E. Pratsinis, A. Baiker, J. Catal. 243 (2006) 229.
[11] M. Piacentini, M. Maciejewski, A. Baiker, Appl. Catal. B: Environ. 66 (2006) 126.
[12] M. Casapu, J.D. Grunwaldt, M. Maciejewski, M. Wittrock, U. Göbel, A. Baiker, Appl. Catal. B: Environ. 63 (2006) 232.
[13] M. Casapu, J.D. Grunwaldt, M. Maciejewski, A. Baiker, S. Eckhoff, U. Göbel, M. Wittrock, J. Catal. 251 (2007) 28.
[14] R. Büchel, R. Strobel, F. Krumeich, A. Baiker, S.E. Pratsinis, J. Catal. 261 (2009) 201.
[15] M. Casapu, J.D. Grunwaldt, M. Maciejewski, A. Baiker, M. Wittrock, U. Göbel, S. Eckhoff, Top. Catal. 42–43 (2007) 3.
[16] D.H. Kim, Y.H. Chin, J.H. Kwak, J. Szanyi, H.F. Peden Charles, Catal. Lett. 105 (2005) 259.
[17] H. Abdulhamid, J. Dawody, E. Fridell, M. Skoglondh, J. Catal. 244 (2006) 169.
[18] H.L. Lin, R.K. Chiang, C.L. Kuo, C.W. Chang, J. Non-cryst. Solids 353 (2007) 1188.
[19] A. Olivera, J. Hafsaoui, J.F. Hochepied, M.H. Berger, A. Thorel, J. Eur. Ceram. Soc. 27 (2007) 3597.
[20] A. Lindholm, N.W. Currier, J. Dawody, A. Hidayat, J. Li, A. Yezerets, L. Olsson, Appl. Catal. B: Environ. 88 (2009) 240.
[21] J.J. Lander, J. Am. Chem. Soc. 73 (1951) 5794.
[22] P. Broqvist, I. Panas, H. Grönbeck, J. Phys. Chem. B 109 (2005) 9613.
[23] P. Broqvist, I. Panas, E. Fridell, H. Persson, J. Phys. Chem. B 106 (2002) 137.
[24] L. Castoldi, I. Nova, L. Lietti, P. Forzatti, Catal. Today 96 (2004) 43.
[25] B.V. L'vov, Thermochim. Acta 303 (1997) 161.
[26] K.V. Tomashevitch, S.V. Kalinin, A.A. Vertegel, N.N. Oleinikov, V.A. Ketsko, Yu.D. Tretyakov, Thermochim. Acta 332 (1998) 101.
[27] B.V. L'vov, V.L. Ugolkov, Thermochim. Acta 410 (2004) 47.
[28] S. Higashimoto, G. Costentin, B. Morin, M. Che, Appl. Catal. B: Environ. 84 (2008) 58.
[29] B. Westberg, E. Fridell, J. Mol. Catal. A 165 (2001) 249.
[30] F. Prinetto, G. Ghiotti, I. Nova, E. Tronconi, P. Forzatti, J. Phys. Chem. B 105 (2001) 12732.
[31] M.O. Symalla, A. Drochner, H. Vogel, S. Philipp, U. Göbel, W. Müller, Top. Catal. 42–43 (2007) 199.
[32] J.P. Breen, R. Burch, C. Fontaine-Gautrelet, C. Hardacre, C. Rioche, Appl. Catal. B: Environ. 81 (2008) 150.
[33] I. Nova, L. Lietti, L. Castoldi, E. Tronconi, P. Forzatti, J. Catal. 239 (2006) 244.
[34] L. Cumaranatunge, S.S. Mulla, A. Yezerets, N.W. Currier, W.N. Delgass, F.H. Ribeiro, J. Catal. 246 (2007) 29.
[35] A. Lindholm, N.W. Currier, E. Fridell, A. Yezerets, L. Olsson, Appl. Catal. B: Environ. 75 (2007) 78.
[36] W.S. Epling, D. Kisinger, C. Everest, Catal. Today 136 (2008) 156.
[37] M. Yang, M. Shen, J. Wang, J. Wen, M. Zhao, J. Wang, W. Wang, J. Phys. Chem. C 113 (2009) 12778.
[38] U. Berner, K. Schierbaum, G. Jones, P. Wincott, S. Haq, G. Thornton, Surf. Sci. 467 (2000) 201.
[39] J. Szanyi, J.H. Kwak, D.H. Kim, X.Q. Wang, R. Chimentao, J. Hanson, W.S. Epling, H.F. Peden Charles, J. Phys. Chem. C 111 (2007) 4678.
[40] H. Yoshida, Y. Yazawa, N. Takagi, A. Satsuma, T. Tanaka, S. Yoshida, S. Hattori, J. Synchrotron Rad. 6 (1999) 471.
[41] D. Bhatia, R.W. McCabe, M.P. Harold, V. Balakotaiah, J. Catal. 266 (2009) 106.
[42] J.P. Breen, C. Rioche, R. Burch, C. Hardacre, Appl. Catal. B: Environ. 72 (2007) 178.
[43] L. Lietti, I. Nova, P. Forzatti, J. Catal. 257 (2008) 270.
[44] N. Le Phuc, E.C. Corbos, X. Courtois, F. Can, P. Marecot, D. Duprez, Appl. Catal. B: Environ. 93 (2009) 12.
[45] Y. Ji, J.S. Choi, T.J. Toops, M. Crocker, M. Naseri, Catal. Today 136 (2008) 146.